Computational limit analysis of soil-arch interaction in masonry arch bridges

M. Gilbert, D.P. Nguyen and C.C. Smith
University of Sheffield, Department of Civil and Structural Engineering, United Kingdom

ABSTRACT**:** The backfill surrounding the arch barrel of a masonry arch bridge can significantly affect its load carrying capacity. However, whilst limit analysis methods are now widely used in assessment, only the arch and piers (if present) are modelled directly in traditional masonry arch bridge limit analysis models. In this paper a holistic computational limit analysis procedure is presented which involves modelling both soil and masonry components explicitly. Masonry bridge parts are discretised using rigid blocks whilst the soil fill is discretised using deformable triangular elements and modelled as a Mohr-Coulomb material with a tension cut-off. Lower and upper bound estimates of the collapse load are obtained. Results are compared with those from a recently performed bridge test carried out in collaboration with the University of Salford; the indication is that it is important to use mobilised rather than peak soil strengths in this type of analysis.

1 INTRODUCTION

Limit analysis methods are now widely used to assess the load carrying capacity of masonry arch bridges (e.g. so called 'line of thrust' and 'mechanism' analysis procedures). Traditionally only the masonry in the arch barrel is considered in the limit analysis model. However, as it has long been established that the surrounding fill can significantly enhance the ultimate load carrying capacity of masonry arch bridges, it appears natural to extend the scope of existing limit analysis models so as to encompass explicit modelling of both arch and fill (in contrast at present most existing arch analysis programs attempt to model the anticipated *effects* of arch fill, rather than the fill itself). Such a holistic computational limit analysis model potentially has distinct advantages over more conventional incremental elasto-plastic finite element models. For example, far fewer input parameters are required and solutions can potentially be obtained rapidly using robust and well developed mathematical programming solvers.

In this paper a holistic computational limit analysis model will be outlined and then used to analyse a full-scale model bridge described elsewhere in the proceedings (Gilbert et al., 2007). In particular the reasonableness of using a rigid-plastic soil model, used in conjunction with a geometrically linear analysis model, will be closely scrutinised.

2 COMPUTATIONAL LIMIT ANALYSIS

Computational limit analysis was first used to identify collapse mechanisms in framed structures some half century ago. Livesley (1978) modified a formulation originally developed for rigid-jointed steel frames to enable problems involving assemblages of rigid blocks to be treated; this approach has since been used to model masonry arch bridges; e.g. it is used in the widely used RING software (http://ring.shef.ac.uk). Recent research has focussed on the development of improved 'non-associative' sliding friction models (e.g. Ferris and Tin-Loi, 2001; Orduna and Lourenco, 2003; Gilbert et al., 2006); however, given the dominance of

hinged mechanisms and other uncertainties, continued use of simpler 'associative' (sawtooth) friction models for masonry arch bridge analysis remains justifiable. Of potentially more importance is the fact that RING and most other masonry arch bridge analysis programs model soil-structure interaction indirectly, according to semi-empirical formulae which have been calibrated against only a small sub-set of the complete family of potential failure modes. This indicates that more realistic modelling of the soil, e.g. as a planar continuum rather than using 1D bar elements for example, would be useful.

For planar continuum problems Maier (1968) and Lysmer (1970) were amongst the first to propose finite element limit analysis problem formulations. Whereas the known, fixed, orientation of joints in masonry block problems enables these to be formulated as linear problems (assuming crushing and non-associative friction are neglected), in continuum problems the relevant yield surface will generally be non-linear. However workers such as Anderheggen and Knopfel (1972) linearised the yield function in a piecewise manner so that linear programming could be employed. Since then many finite element limit analysis formulations have been proposed, with geomechanics being a particularly popular application (e.g. Sloan, 1988). However, the focus has generally been confined to limit analysis of the soil elements only. As a notable exception, Cavicchi and Gambarotta (2005) recently presented an upper bound finite element limit analysis model of the soil-arch interaction problem, which is also considered here. However, the masonry was represented using 1D beam elements (rather than using more realistic 2D masonry blocks) and relatively inaccurate constant strain elements were employed in the finite element model of the soil. This paper aims to address both these shortcomings, and to also tightly bound the true solution from both above and below. Additionally, results from the model developed will be compared with experimental data gleaned from a carefully controlled laboratory test, described elsewhere in the proceedings (Gilbert et al., 2007).

In the following section the essential details of the numerical model developed are briefly outlined.

3 NUMERICAL MODEL OF MASONRY-SOIL INTERACTION

3.1 Model of masonry parts

The constituent masonry blocks are assumed to be rigid, with failure (rocking and/or sliding) occurring only in the joints between units. The constraints needed for both equilibrium and kinematic (work) formulations follow.

3.1.1 Equilibrium formulation

Contact and block forces, dimensions and frictional properties are shown on Fig. 1. The problem variables are the contact forces: n_i, s_i, m_i (where $n_i \geq 0$; s_i, m_i are unrestricted 'free' variables), and the unknown collapse load factor λ.

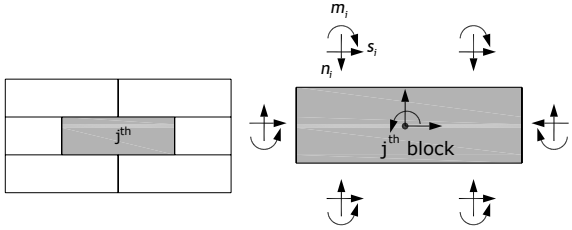

Figure 1 : Typical block assemblage

Assuming there are *b* blocks and *c* contact surfaces, equilibrium (1) and yield constraint (2) equations may be stated for the problem as follows:

$$\mathbf{B}_{\mathrm{m}}\mathbf{q}_{\mathrm{m}} - \lambda \mathbf{f}_{\mathrm{m}L} = \mathbf{f}_{\mathrm{m}D} \tag{1}$$

$$\mathbf{C}_{\mathrm{m}}^{\mathrm{T}}\mathbf{q}_{\mathrm{m}} \le \mathbf{0} \tag{2}$$

where $\mathbf{B}_{\mathrm{m}}$ is a suitable ($3b \times 3c$) equilibrium matrix for the masonry containing direction cosines and $\mathbf{q}_{\mathrm{m}}$ and $\mathbf{f}_{\mathrm{m}}$ are respectively vectors of contact forces and block loads. $\mathbf{f}_{\mathrm{m}} = \mathbf{f}_{\mathrm{m}D} + \lambda\mathbf{f}_{\mathrm{m}L}$ where $\mathbf{f}_{\mathrm{m}D}$ and $\mathbf{f}_{\mathrm{m}L}$ are respectively vectors of dead and live loads and $\mathbf{q}_{\mathrm{m}}^{\mathbf{T}} = \left\{n_1, s_1, m_1, n_2, s_2, m_2, \ldots n_c, s_c, m_c\right\}$, with applied loads at the block centroids (nodes). $\mathbf{C}_{\mathrm{m}}$ is a suitable yield constraint matrix. In the present study equation (2) simply imposes the familiar sliding yield constraint: $|s_i| \le n_i \tan\phi_i$ and rocking yield constraint $|m_i| \le 0.5 n_i t_i$, for each contact, $i = 1, \ldots, c$.

3.1.2 Kinematic formulation

The kinematic formulation may be derived using duality principles and can be stated as:

$$\mathbf{f}_{\mathrm{m}L}^{\mathrm{T}}\mathbf{d}_{\mathrm{m}} = 1 \tag{3}$$

$$\mathbf{B}_{\mathrm{m}}^{\mathrm{T}}\mathbf{d}_{\mathrm{m}} - \mathbf{C}_{\mathrm{m}}\mathbf{p}_{\mathrm{m}} = \mathbf{0} \tag{4}$$

$$\mathbf{p}_{\mathrm{m}} \ge \mathbf{0} \tag{5}$$

where $\mathbf{d}_{\mathrm{m}}$ is a $3b$-vector of nodal unconstrained displacements corresponding to the nodal loads $\mathbf{f}_{\mathrm{m}}$ and where resultant displacements in $\mathbf{p}_{\mathrm{m}}$ correspond to the contact forces in $\mathbf{q}_{\mathrm{m}}$ in a virtual work sense (note that for simplicity the terms displacement and energy dissipation are here used as shorthand for displacement rate and rate of energy dissipation).

3.2 Model of soil

3.2.1 Equilibrium formulation (lower bound approach)

Following the approach of Sloan (1988), the soil is discretised using three-noded linear-stress elements separated by discontinuities. Each node in a triangular element therefore has three unknown stresses (σ_x, σ_y, τ_{xy}), which are constrained so as to satisfy (linear) equilibrium and (nonlinear) yield constraints. Linear programming (LP) can however be applied if the Mohr-Coulomb failure envelope is approximated by a polygon. Unlike Sloan (1988), here the yield surface is instead approximated with an exterior polygon and then adaptively refined using an efficient iterative LP solution scheme which terminates when no stresses violate yield, thereby ensuring the true (nonlinear) yield surface is enforced.

3.2.2 Kinematic formulation (upper bound approach)

The soil is discretised using six-noded linear strain elements with straight sides. The apex of each triangular element is associated with a specified number of plastic multipliers. This allows the soil behaviour to be modelled more accurately than when using lower order elements (e.g. the three-noded constant strain elements used by Cavicchi and Gambarotta 2005). It also avoids the locking problem discussed by Nagtegaal et al. (1974) without the need to resort to special arrangements of elements within the mesh. Each node is unique to its element, permitting displacement jumps to be modelled at inter-element boundaries. A kinematically admissible velocity field will be obtained provided the associative flow rule is enforced both within elements and along discontinuities (Makrodimopoulos and Martin 2006); the displacement boundary condition should also be enforced. The upper bound collapse load can then be obtained by minimising the internal energy dissipation, set to be equal to the work done by the external applied loads.

3.3 Model of soil-masonry interface

3.3.1 Equilibrium formulation (lower bound approach)

Given that the soil model is formulated in terms of stresses whereas the masonry block model is formulated in terms of stress-resultants (i.e. forces) all that remains is to define a suitable equilibrium relationship at the soil-masonry interface:

$$\mathbf{A}_s\boldsymbol{\sigma}_s - \mathbf{q}_m = \mathbf{0} \tag{6}$$

where $\boldsymbol{\sigma}_s$ contains normal and shear stresses at the interface and $\mathbf{A}_s$ is a suitable transformation matrix. Also yield constraints are imposed as in equation (2), though with $\mathbf{C}_m$ replaced by $\mathbf{C}_{sm}$, which contains the relevant soil-masonry interface coefficients.

3.3.2 Kinematic formulation (upper bound approach)

The kinematic formulation for a soil-masonry interface is given by:

$$\mathbf{Q}_{sm}\mathbf{d}_{sm} - \mathbf{C}_{sm}\mathbf{p}_{sm} = \mathbf{0} \tag{7}$$

$$\mathbf{p}_{sm} \geq \mathbf{0} \tag{8}$$

$$\mathbf{M}_s\mathbf{d}_s = \mathbf{0} \tag{9}$$

where $\mathbf{Q}_{sm}\mathbf{d}_{sm}$ and $\mathbf{C}_{sm}\mathbf{p}_{sm}$ represent suitable soil-masonry compatibility and flow rule constraints respectively. It is also necessary to prescribe that the discontinuities should vary linearly so that the discontinuities displace compatibly with the masonry displacement; this can be satisfied by imposition of (9), where $\mathbf{d}_s$ contains soil displacements at the interface and $\mathbf{M}_s$ is a suitable enforcement matrix.

3.4 Solution

The problems may be solved using linear programming, either maximising λ in the case of the equilibrium formulation, or minimising the work done by dead loads and internal energy dissipation in the kinematic formulation.

4 APPLICATION OF NUMERICAL MODEL TO A LABORATORY BRIDGE

As well as developing numerical soil-arch interaction models, the authors are in parallel involved in carrying out physical model tests on full-scale 3m span soil-filled masonry arch bridges (Gilbert et al., 2007). Key benefits of using test data from these bridges to verify the numerical model are that: (i) the characteristics of the constituent materials are known, (ii) the bridges are being tested under plane strain conditions, replicating those in the model. In this paper experimental data from a 3m span arch bridge backfilled with crushed limestone is compared with results obtained using the numerical model.

Material properties for this test were determined as follows: soil: effective cohesion $c' = 3.3\text{kN/m}^2$, effective angle of friction $\phi' = 54.5°$, unit weight $\gamma = 19.1\ \text{kN/m}^3$; Masonry: joint angle of friction $\phi = 31°$, $\gamma = 23.7\ \text{kN/m}^3$. The soil properties were obtained from 300 × 300mm shear box tests carried out at normal stresses of 25 kPa and 100 kPa, employing 3 repeat tests for each stress level. The soil-masonry interface angle of friction δ, has not yet been measured experimentally and was initially taken as $1/3\phi'$. This is based on the Eurocode 7 recommendation of taking $\delta = 2/3\phi'_{cv}$ for the interface between sand/gravel and precast concrete, where ϕ'_{cv} is the critical state angle of friction of the soil. Although critical state values were not available from the shear box tests, they might be expected to be significantly lower than the peak strength. Additionally for simplicity the base of the loading beam was modelled as being

'smooth'. Similar though not identical meshes comprising 8132 and 8121 elements were used for the upper and lower bound analyses respectively. The meshes were manually refined around the base of the surface load and a relatively fine mesh was used around the arch barrel to capture the essential features of the soil-arch interaction. Initial simulations showed that the associative flow rule used for the soil backfill led to unreasonably high stresses at the left hand side abutment, due to excessive dilation. To reduce this effect, the soil-arch interface friction δ for the first 4 voussoirs was taken as zero (this had a negligible effect on the overall collapse load). Results from initial upper bound (UB1) and lower-bound (LB1) models are given in Figs. 2-5.

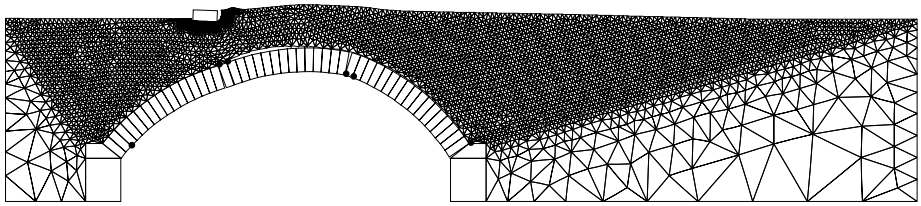

Figure 2 : Deformed shape of soil and arch (UB1)

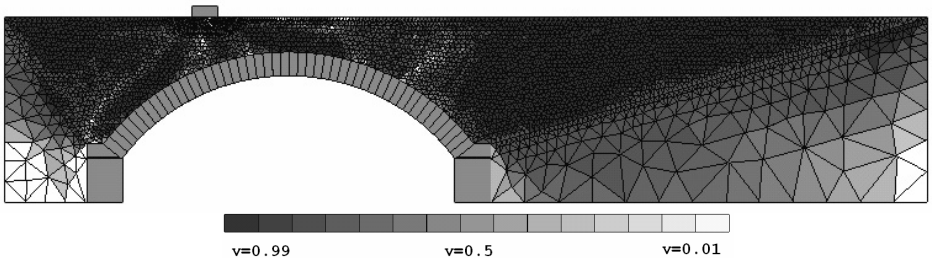

Figure 3 : Variation in maximum shear stress relative to the yield stress (LB1)

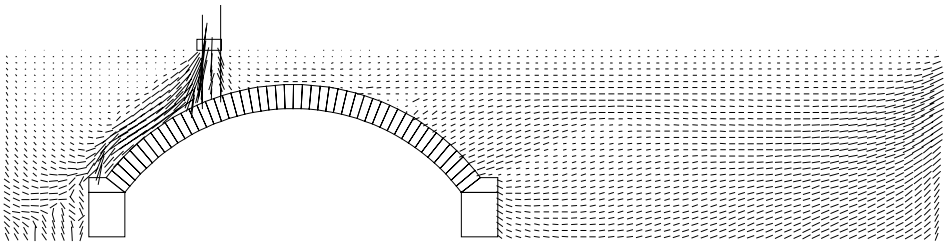

Figure 4 : Maximum (compressive) principal stress vectors (LB1)

In both model and experiment, the arch collapsed in a classic 4 hinge mechanism, as shown in Fig. 2 (though it is evident that in some areas 'diffused' hinges formed). Figure 3 indicates the presence of yielding soil (dark shaded areas) both under the load and in the soil around the 'passive' right hand side of the arch, where the arch barrel sways into the soil mass. Figure 4 indicates that the stresses 'flow' in two 'streams', the right hand stream focussing load directly onto the arch extrados, just to the right of the loading beam, and the left hand 'stream' taking the stresses almost parallel to the arch extrados towards the abutments. The net effect can be seen in Fig. 5 which shows that the load focuses both to the left and right of the surface load. On the passive side there is a gradual increase in normal and shear stress with depth. The initial predicted lower bound load carrying capacity (LB1) was 181kN, which is significantly greater than the experimental peak load (both are plotted in Fig. 6; also shown is the upper bound, UB1). Four main factors can be considered as contributing to this gross over-prediction:

(i) Soil strength is only mobilised by large deformations, an effect which needs to be considered separately on each side of the arch.
(ii) Soil/arch interface properties were estimated rather than measured.
(iii) The loading beam friction was assumed to be smooth as a measured value was unavailable.
(iv) Gross displacements of the arch cause it to lose strength.

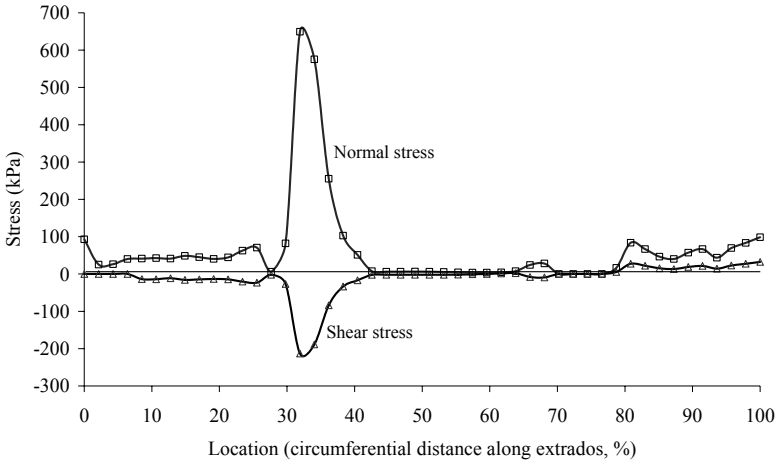

Figure 5: Shear and normal stresses on the extrados (LB1), $\delta/\phi' = 0.33$

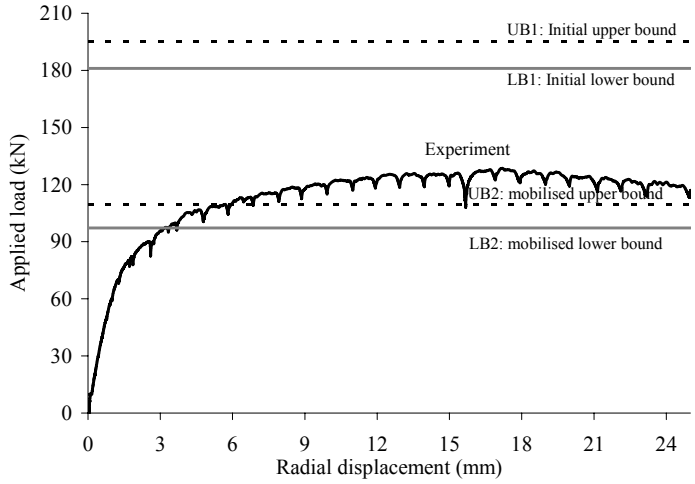

Figure 6: Predicted and experimental load vs. displacement responses for masonry bridge (LB1, UB1: $M = 1$, $F = 0.33$, $P = 0$; LB2, UB2: $M = 0.25$, $F = 0.33$, $P = 0$)

To identify the relative significance of each of the first three parameters, a parametric study was performed. Taking the parameter set described previously as the benchmark, the influence of varying individual parameters was investigated (the small value of c' for the soil was, for sake of simplicity, kept constant). The parameter M describes a soil mobilisation factor such that the mobilised value of soil friction ϕ_{mob} employed in the analysis is given by $\phi_{mob} = M\phi'$ (where $\phi' = 54.5°$ in this study). The parameter F describes the ratio δ/ϕ_{mob}, where δ is the soil-arch interface friction, and the parameter P describes the ratio δ/ϕ_{mob}, where δ is the soil-loading beam interface friction.

It is evident from Fig. 7 that the loading beam friction has negligible influence on load capacity, in contrast to the considerable influence of base friction in the case of ordinary foundation footings. This appears logical in that most soil movement and transfer of load is directly downwards in the arch problem, rather than laterally in the case of a foundation footing problem.

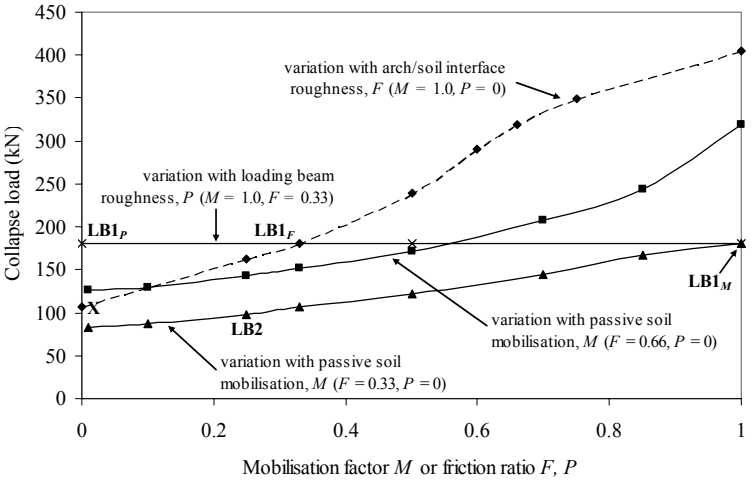

Figure 7: Variation in ultimate load capacity (lower bound) with different soil/arch interface properties, soil mobilisation factors and platen base friction properties. Soil mobilisation factors were applied only to passive side of arch (letters in brackets indicate the parameter plotted on the x-axis).

In contrast, the soil/arch interface properties can be seen to have a very significant effect on predicted load carrying capacity. A close match between experiment and model is only achieved if an almost perfectly smooth interface is assumed (point X in Fig. 7), which does not seem reasonable. Conversely, taking $F = 0.33$ gives a high predicted capacity for full soil mobilisation (Point $LB1_F$ in Fig. 7). It is therefore necessary to investigate the effects of soil strength mobilisation and gross displacements. The relative importance of these can be considered if the shear strain in the soil caused by a given movement of the arch mechanism is estimated. In this failure mechanism a 1 mm displacement under the load corresponds approximately to a 0.1% arch segment rotation on the passive side and approximately to a 0.1% shear strain in the adjacent soil. Thus as the load-displacement curve in Fig. 6 starts to enter the plastic region at a displacement of approx. 1.0mm, , this corresponds to ~ 0.1% strain in the limestone. Based on the shear box data, this in turn corresponds to a mobilisation of $M \approx 0.25$, and to a predicted collapse load of just under 100 kN, as indicated in Fig. 6 (labelled LB2; also shown in Fig. 7).

Based on investigations reported by Gilbert (1997), an arch of the same geometry as considered here but with no backfill is likely to reach its peak load carrying capacity at a radial displacement under the load of ≈ 1mm. At larger displacements the load carrying capacity progressively reduces, and a gross displacement (i.e. geometrically non-linear) analysis is ideally required. In the test bridge considered here the peak load carrying capacity was achieved at a displacement of approx. 17mm, or ≈ 2% shear strain, which should generate a fully mobilised limestone strength ($M = 1.0$). Gilbert (1997) showed that this level of deflection would reduce the arch load carrying capacity to approx. 60% of its initial value. It is notable that taking 60% of the initial predicted capacities (i.e. LB1, UB1 shown in Fig. 6) leads to much more reasonable predictions of the experimentally observed load carrying capacity.

It should be emphasised that the aforementioned numerical figures are approximate, and our intention has been to explore the likely contributions of the factors involved, thereby informing future research. Additionally the effect of soil strength mobilisation has only been investigated on the 'passive' side, and not on the 'active' side, where the interactions are potentially rather more complex.

5 CONCLUSIONS

- Upper and lower bound computational limit analysis models have been developed for soil-arch interaction problems. Use of quadratic displacement elements for the soil in the upper bound model improves upper bound predictions and reasonably close bounds on the theoretical 'exact' collapse load have been obtained.
- Some difficulties were initially experienced when attempting to apply the model to a laboratory test bridge. Although high quality soil strength data was available, since soil strength requires significant strains before it is fully mobilised, there were question-marks over what values should be used in the model, given also that large arch deformations reduce its load carrying capacity. Furthermore the soil-arch interface friction has not yet been measured, introducing further uncertainty.
- Numerical results indicate that the nature of the surface load (smooth or rough) has negligible effect on the arch load capacity, whilst in contrast the soil/arch interface properties have a significant influence on the predicted ultimate load carrying capacity.
- To address the strength mobilisation issue, the use of strength mobilisation factors has been investigated, basing these on the strength at a given anticipated soil strains.
- Though further investigations are warranted it is now clear that neglecting soil strength mobilisation and/or gross displacement strength reduction may lead to significant over-prediction of the ultimate collapse load.

ACKNOWLEDGEMENTS

The authors wish to acknowledge the support of the UK Engineering and Physical Sciences Research Council (EPSRC), under grant references GR/S53329/01 and GR/S53336/01.

REFERENCES

Anderheggen, D., Knopfel, H. 1972, Finite element limit analysis using linear programming, *International Journal Solids and Structures.* 3, p. 1413-1431.

Cavicchi, A., Gambarotta, L. 2005. Collapse analysis of masonry bridges taking into account arch–fill interaction. *Engineering Structures.* 27, p. 605-615.

Ferris, M.C., Tin-Loi, F., 2001. Limit analysis of frictional block assemblies as a mathematical program with complementarity constraints. *International Journal of Mechanical Sciences*. 43, p. 209-224.

Gilbert, M. 1997. Gross displacement mechanism analysis of masonry bridges and tunnel linings. *Proceedings of the 11th International Brick/Block masonry conference*. Shanghai, p. 473-482.

Gilbert, M., Casapulla, C., Ahmed, H.M., 2006. Limit analysis of masonry block structures with non-associative frictional joints using linear programming. *Computers and Structures*. 84, p. 873-887.

Gilbert M., Nguyen D., and Smith, C.C. 2007. Computational limit analysis of soil-arch interaction in masonry arch bridges. *Proc. 5th International Arch Bridges Conference*, Madeira.

Livesley, R.K. 1978, Limit analysis of structures formed from rigid blocks. *International Journal of Numerical Methods in Engineering*, 12. p. 1853-1871.

Lysmer, J. 1970, Limit analysis of plane problems in soil mechanics, *ASCE Journal of Soil Mechanics and Foundations Division*. 96, p. 1311-1334.

Maier, G. 1968, Quadratic programming and theory of perfectly plastic structures, *Meccanica*, 3, p. 265-273.

Makrodimopoulos, A. Martin, C.M. 2006 Advances in numerical upper bound limit analysis. *Proc. International Conference in Memoriam of Prof. P.D. Panagiotopoulos*, Thessaloniki, Greece, p. 213-220.

Nagtegaal, J., Parks, D., Rice, J. 1974. On numerically accurate finite element solutions in the fully plastic range. *Comput. Methods Appl. Mech. Engrg.* 4, p. 153-177.

Orduna, A., Lourenco, P. 2003. Cap Model for Limit Analysis and Strengthening of Masonry Structures *Journal of Structural Engineering*. 129, p. 1367-1375.

Sloan, S. 1988. Lowerbound limit analysis using finite elements and linear programming. *International Journal of Numerical and Analytical Methods in Geomechanics.* 12, p. 61-77.

Sloan, S., Kleeman, P. 1995. Upper bound limit analysis using discontinuous velocity fields. *Comp. Meths Appl. Mech. Engrg.* 127, p. 293-314.